



OPEN ACCESS

EDITED BY

Xander Wang,
University of Prince Edward Island,
Canada

REVIEWED BY

Karoly Nemeth,
Institute of Earth Physics and Space
Sciences, Hungary
Ning Chen,
Lanzhou University, China

*CORRESPONDENCE

Uri Basson,
✉ ubasson@gmail.com

RECEIVED 26 February 2023

ACCEPTED 27 June 2023

PUBLISHED 14 July 2023

CITATION

Basson U, Argaman E, Yizhaq H, Xu C,
Xu Z and Stavi I (2023), Subsurface
geodiversity determines shrub resilience
vs. mortality under long-term droughts in
the Israeli Negev drylands.

Front. Environ. Sci. 11:1168104.
doi: 10.3389/fenvs.2023.1168104

COPYRIGHT

© 2023 Basson, Argaman, Yizhaq, Xu, Xu
and Stavi. This is an open-access article
distributed under the terms of the
[Creative Commons Attribution License
\(CC BY\)](https://creativecommons.org/licenses/by/4.0/). The use, distribution or
reproduction in other forums is
permitted, provided the original author(s)
and the copyright owner(s) are credited
and that the original publication in this
journal is cited, in accordance with
accepted academic practice. No use,
distribution or reproduction is permitted
which does not comply with these terms.

Subsurface geodiversity determines shrub resilience vs. mortality under long-term droughts in the Israeli Negev drylands

Uri Basson^{1,2*}, Eli Argaman³, Hezi Yizhaq⁴, Chi Xu⁵, Zhiwei Xu⁶
and Ilan Stavi^{7,8}

¹GeoSense Ltd., Even-Yehuda, Israel, ²Department of Marine Geosciences, School of Marine Science, University of Haifa, Haifa, Israel, ³Soil Erosion Research Station, Ministry of Agriculture & Rural Development, Bet Dagan, Israel, ⁴Department of Solar Energy and Environmental Physics, Blaustein Institute for Desert Research, Ben-Gurion University of the Negev, Sede Boqer Campus, Be'er Sheva, Israel, ⁵School of Life Sciences, Nanjing University, Nanjing, China, ⁶School of Geography and Ocean Science, Nanjing University, Nanjing, China, ⁷Dead Sea and Arava Science Center, Yotvata, Israel, ⁸Ben-Gurion University of the Negev, Eilat Campus, Eilat, Israel

Shrubs, encompassing important ecosystem engineers in dryland environments, have experienced mass mortality due to long-term droughts across the northwestern Israeli Negev. This massive die-back, which has particularly affected the predominant shrub species *Noaea mucronata*, predominates edaphically homogeneous (low geodiversity) hillslopes, and is minor in edaphically heterogeneous (high geodiversity) hillslopes. While the homogeneous hillslopes encompass a thick and non-stony soil layer, the heterogeneous hillslopes are composed of a thin, stony layer that overlies weathered, chalky bedrock. The objective of this geophysical study was to assess the subsurface and bedrock characteristics, and its effect on shrub durability vs mass mortality in a dryland ecosystem. A combination of 2D and 3D Ground Penetrating Radar (GPR) imaging and Frequency Domain Electromagnetics (FDEM) was applied. For the GPR procedure, the 2D and 3D reflection imaging was dominated by different dielectric permittivities (dielectric constants) of layers and changes in soil-rock-water content. For the FDEM procedure, the soil-rock electrical properties, alongside the concentration of dissolved salts, determined the measured electrical conductivity (EC). The results show substantial differences in EC values between the homogeneous and heterogeneous hillslopes, which are attributed to differences in the soil-rock interface, soil-water content, and salts concentration. Overall, the much greater EC values of the soil-rock interface in the heterogeneous hillslopes are expected to adversely affect shrub vitality. However, the greater shrub vitality in these hillslopes is likely attributed to the fractured and weathered chalky underground, which retains moisture in pockets or micro-aquicludes that increase water availability for the shrubs. Under these better habitat conditions of the heterogeneous hillslopes, the high EC values do not limit shrub survival or growth. At the same time, the absence of such water pockets in the thick soil layer of the homogeneous hillslopes imposes severe stress under long-term drought conditions, resulting in shrub die-off. This study illustrates the vital role of subsurface geodiversity in determining the resilience of dryland ecosystems to droughts and climatic change.

KEYWORDS

climate change, geo-ecosystem functioning, soil quality, soil/rock-water availability, subsurface features, underground properties

Introduction

Geodiversity—the natural heterogeneity of geological, geomorphic, and soil characteristics—demonstrates the complexity of natural systems (Gray, 2005). Measuring geodiversity may be implemented qualitatively, quantitatively, or using combined qualitative-quantitative methods. Through regulating the ecosystem's physical conditions, geodiversity affects biodiversity, specifically plant diversity (Ibáñez et al., 2016; Crisp et al., 2022). During the last decade, geodiversity has been extensively studied in the context of ecosystem functions and services (Summers et al., 2018). Specifically, close relationships exist between geodiversity and hydrological connectivity (Calvo-Cases et al., 2021), with consequent implications for water overland flow and subsurface storage. Many studies have focused on relatively large spatial scales spanning between hillslope and watershed scales (e.g., Thomas, 2012; Alahuhta et al., 2019; Bétard and Peulvast, 2019; dos Santos et al., 2019). Recently, many studies have focused on comparatively small spatial scales, specifically on the vegetation-patch and sub-patch scales (Stavi et al., 2018b; Stavi et al., 2019). Among the geodiversity-related topics, an emphasis has been recently given to the impact on resource availability under resource-limited conditions, e.g., soil-water availability in drylands (Stavi et al., 2018b; Stavi et al., 2021b).

Notably, the impact of geodiversity on vegetation's resilience under long-term and frequent droughts has been assessed, demonstrating the potential effect of geodiversity in alleviating plant-water stress (Stavi et al., 2018a; Stavi et al., 2021a). Although this effect has not been empirically assessed, it was suggested to be related to the ability of woody vegetation with characteristic deep root systems to penetrate through fractured rocks and reach comparatively deep soil-water (Stavi et al., 2019; Stavi et al., 2021b). For example, such an effect was proposed for several oak (*Quercus*) species under the hot and dry Mediterranean climatic conditions in northern Israel (Herr et al., 2016) and in the western United States (Hellmers et al., 1955; Davis, 1977; Hahm et al., 2020). A recent study showed the extensive prevalence of rock-water use by woody plants across the United States, with predominance for arid, semi-arid, and Mediterranean climatic regions (McCormick et al., 2021).

Since the turn of the 21st century, the semiarid northwestern Negev of Israel—along with extensive areas of the southern Levant—has faced a period of consecutive drought events (EcoPeace Middle East, 2019). Following the severe drought of 2008–2009, the predominant shrub species, *Noaea mucronata* (Forssk.) Asch. and Schweinf, experienced mass mortality throughout the Sayeret Shaked Long Term Ecological Research (LTER) Park (Shachak, 2011; Sher et al., 2012; Zaady et al., 2012). However, recent studies reported that the response of this shrub species to the stress conditions is site-specific and dependent on landform type. In particular, these studies showed that the mass mortality occurred in low-geodiversity (homogeneous) hillslopes with a thick soil profile and no stoniness throughout the soil profile (Stavi et al., 2021a; Stavi et al., 2021b). At the same time, this shrub

species has thrived in high-geodiversity (heterogeneous) hillslopes, characterized by a highly-weathered bedrock layer overlain by a thin layer of stony soil, and with a high cover of rock fragments on the ground surface (Stavi et al., 2018a; Stavi et al., 2019; Stavi et al., 2021a). Despite these recent observations, the specific mechanism that enables these shrubs to thrive in the heterogeneous hillslopes is still unclear.

The objective of this study was to explore this mechanism through a three-dimensional detection of the subsurface substance of homogeneous and heterogeneous hillslopes in Sayeret Shaked LTER Park, using geophysical exploration methods of Frequency Domain Electromagnetics (FDEM) and Ground Penetrating Radar (GPR). In order to inspect subsurface properties, an extensive geophysical, high-resolution and multidimensional analysis of the subsurface was implemented utilizing state-of-the-art imaging and geospatial mapping methodologies. The exploration was conducted to determine several factors - —a) soil-rock stratigraphic settings; b) the degree and pattern of bedrock fracturing; c) the subsurface's relative volumetric soil-water content; and d) the subsurface's relative electrical conductivity (EC). Integrating FDEM and GPR methods to assess subsurface geodiversity and its implications for dryland ecosystems, as orthogonal complementary means, is a novel approach. The study hypothesis was that shrub mortality in the homogeneous hillslopes is due to severe stress conditions imposed by the low soil-water availability, whereas shrubs in the heterogeneous hillslopes reach deep-stored high-moisture pockets (micro-aquicludes) through cracks and fractures in the highly weathered underground rock layer.

Materials and methods

Regional settings

Sayeret Shaked Park (31°27'N, 34°65'E; 187 m. a.s.l.), spanning ~600 ha, is located in the semiarid northwestern Negev of Israel (Figure 1). Mean daily temperatures in the coldest (January) and warmest (July) months are 12°C and 26°C, respectively. Until the end of the 20th century, the mean annual long-term precipitation was 200 mm (<https://ims.gov.il/he/ClimateAtlas>). Since then, it has dropped to ~150 mm y⁻¹, with high interannual variability (Argaman et al., 2020). The region's lithology comprises chalk of the Eocene and Plio-Pleistocene eolianites (aeolian deposits). The predominant soil is classified as loessial calcic xerosol, with a sandy loam to loamy sand texture (Stavi et al., 2018; 2019; 2021b). The native vegetation community comprises shrubs, herbaceous plants, and geophytes. The predominant shrub species is *N. mucronata*, with *Helianthemum kahiricum* Delile and *Anabasis articulata* (Forssk.) Moq also being prevalent. In 1989, ~40 ha of the park were declared as a LTER site and fenced to prevent livestock access (Stavi et al., 2018a; Stavi et al., 2019; Argaman et al., 2020).

Mass mortality of *N. mucronata* shrubs across the region was initially reported over a decade ago and was attributed to the

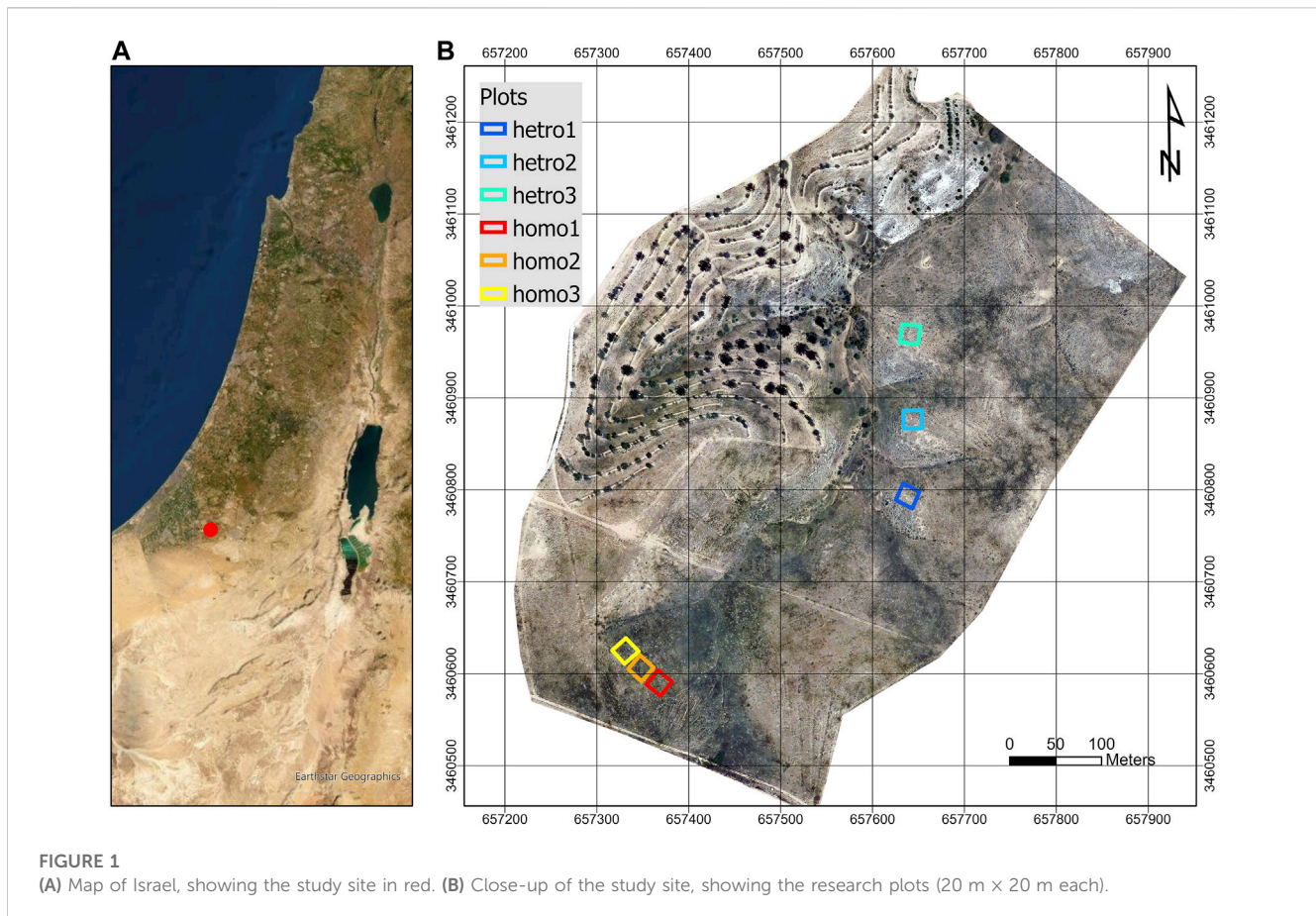


FIGURE 1
(A) Map of Israel, showing the study site in red. (B) Close-up of the study site, showing the research plots (20 m x 20 m each).

long-term droughts since the turn of the century (Shachak, 2011; Sher et al., 2012). Yet, a detailed survey of the LTER park revealed that shrub mortality is confined to homogeneous hillslopes, i.e., hillslopes with a homogeneous thick (>1 m) soil layer lacking stones in the soil profile and on the ground surface. At the same time, negligible shrub mortality was observed in heterogeneous hillslopes, i.e., hillslopes with a thin (~0.1 m) soil layer overlying a highly-weathered bedrock layer and with a considerable (~30%) stoniness in the soil profile and on the ground surface (Stavi et al., 2018a; Stavi et al., 2019; Stavi et al., 2021a). Vegetation and soil data according to hillslope type are presented in Table 1.

The utilized methods

The FDEM is a non-destructive remote sensing and active geophysical method used for high-resolution “potential method” characterization and mapping of shallow subsurface structures and targets. The system’s functionality is primarily based on how the electrical conductivities and magnetic susceptibilities of different materials respond to changing magnetic fields. These fields, generated by the system, induce eddy currents within the materials (Figure 4). The GPR is a non-invasive “reflection” geophysical method used for high-resolution imaging and mapping of shallow subsurface structures (Basson et al., 1994; Basson, 2000; Basson et al., 2002; Basson and Ginzburg, 2008; Basson, 2020; Baruch et al., 2021; Basson, 2021; Lazar et al.,

2021). The method’s functionality is based on the differences in electromagnetic properties of the subsurface materials and their reactions to propagating EM waves (Ulriksen, 1982; Davis and Annan, 1989). The GPR uses high-frequency EM waves to detect changes in subsurface properties, including dielectric permittivity, electric conductivity, and magnetic permeability. The GPR antennas send and receive EM waves, recording the returning waves over a selectable time window. These waves propagate at different velocities, allowing the computation of depths and distances to subsurface targets. Velocity analysis also forms the basis for moisture content calculations (Basson, 2000) (see Supplementary Appendixes I, II for additional information about the FDEM and GPR technologies).

The FDEM and GPR methods were used in the study (Figures 2–4) as complementary methods that allow non-invasive exploration of the subsurface. As such, the FDEM and GPR techniques are used in many study areas, such as geology, sedimentology, hydrology, environmental science, archaeology, civil engineering, tectonics, and more (Davis and Annan, 1989; Basson et al., 1994; Basson, 2000; Basson et al., 2002; Lazar et al., 2021). The GPR method involves transmitting high-frequency electromagnetic waves (EMW) into the ground to detect changes in electromagnetic subsurface properties. These include dielectric permittivity, electric conductivity, and magnetic permeability, which are a function of soil and rock materials, soil-water content, and other subsurface features, which can be measured as a function of location and depth (Figure 3). The FDEM method involves

TABLE 1 Vegetal and physical properties according to hillslope type.

Hillslope type	Heterogeneous			Homogeneous		
	Alive	Dead	Total	Alive	Dead	Total
<i>Noaea mucronata</i>	12.1 (1.8)	0.8 (0.2)	12.9 (1.7)	0.3 (0.2)	5.3 (0.8)	5.6 (0.6)
<i>Deverra tortuosa</i>	0.3 (0.1)	NA	0.3 (0.1)	1.9 (1.6)	NA	1.9 (1.6)
<i>Helianthemum kahiricum</i>	7.8 (2.3)	0.6 (0.2)	8.4 (2.3)	NA	NA	NA
<i>Echinops polyceras</i>	1.5 (0.6)	NA	1.5 (0.6)	NA	NA	NA
<i>Anabasis articulata</i>	2.5 (1.7)	NA	2.5 (1.7)	NA	NA	NA
<i>Phagnalon rupestre</i>	0.7 (0.3)	NA	0.7 (0.3)	NA	NA	NA
Total shrubby vegetation	24.9 (4.0)	1.4 (0.2)	26.3 (4.1)	2.2 (1.8)	5.3 (0.8)	7.5 (1.1)
Physical properties			Total			Total
Partially-embedded rock fragments			18.9 (1.1)			NA
Resting rock fragments			4.2 (0.7)			NA
Total rock fragments			23.1 (1.6)			NA
Exposed soil			18.8 (1.2)			NA
Faunal perturbation			1.4 (0.8)			NA
Geophytes			0.7 (0.3)			NA
Herbaceous vegetation			29.7 (2.0)			92.5 (1.1)
Total cover (%)			123.1 (7.4)			100.0 (0.0)

Notes: NA, not available. Numbers within parentheses are standard errors of the means. Total cover (in the heterogeneous hillslopes) is >100% due to the line-point intercept method of the transect survey, allowing documentation of more than one layer in the same spot. Modified from Stavi et al. (2018a).

generating primary alternating magnetic fields that induce alternating electrical eddy currents into the ground, resulting in secondary magnetic fields due to interaction with the internal ground (Figure 4). The relations between the alternating magnetic fields are proportional to the subsurface/target electrical conductivity and magnetic susceptibility. These methods have become standard applicative tools used to investigate various environmental and engineering issues (ASTM International, 2023a and its active standard replacement ASTM International, 2023b; ASTM International, 2023c). For more information and references on these methods see Supplementary Appendixes I, II. The measurements across Sayeret Shaked Park were conducted by combining the FDEM and the GPR methods, as described by the top-view shown in Figure 5. The penetration depths of the FDEM/Gem-2 sensors are a function of their design, operating frequency, and subsurface EM properties. In Table 2 we present the penetration depth vs frequency for our study.

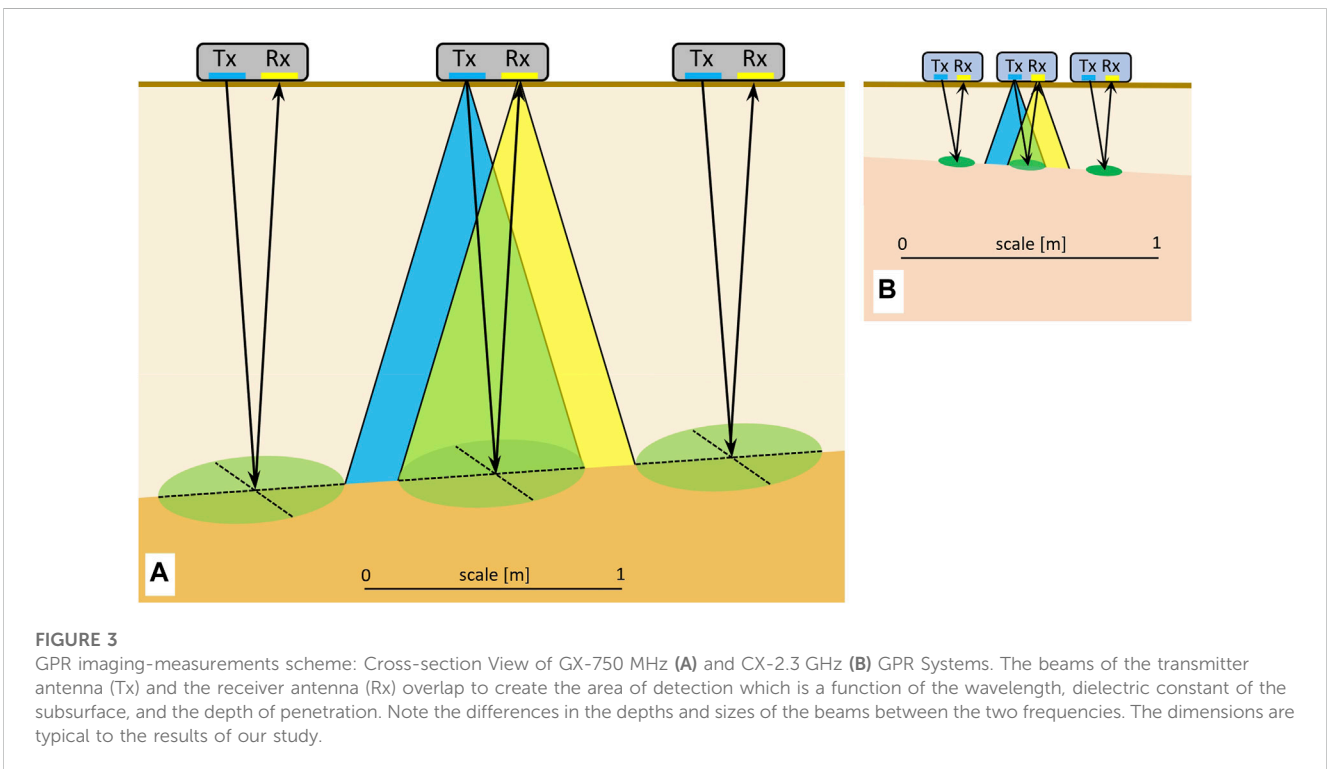
Description of technologies and measurements setting

The geophysical exploration was planned based on the expected lithology described by Stavi et al. (2018a), Stavi et al. (2019), Stavi et al. (2021b). To cover a variety of depths and resolution capabilities for imaging and mapping, we applied a wide range of frequencies using two different GPR systems of MALÅ GeoScience AB

(Figure 3). This range allows near real-time sampling and hyperstacking, lowering the threshold of signal-to-noise ratio and broader bandwidth, i.e., providing higher resolution. The Ground Explorer (GX) has a medium-resolution of 750 MHz antennae, and the Concrete Explorer (CX) has a high-resolution 2.3 GHz antenna, allowing a clear differentiation between soil horizons. The imaging parameters, settings, and average EMW velocities of the measurements used (on 5 April 2021) in this study are described in Table 3.

The particular combination of the two different frequencies/GPR systems used in this study allowed us to utilize a two-resolution approach, with a) medium-resolution high-clarity 2D imaging using the HDR GPR GX-750 MHz to an average depth of ~1.4 m over a relatively wide area of 5 m × 3 m, and b) high-resolution 3D imaging using the GPR CX-2.3 GHz to an average depth of ~0.3 m over an area of 0.8 m × 0.8 m (Figures 4, 6). The GPR measurements of soil-water content of the homogeneous hillslopes were based on the velocity analysis results, as well as on the soil texture data. Dielectric permittivities of the soil were computed from the measured velocities of the EMW, with a constraint for the driest layer near the surface and additional moisture-content levels that were computed for the relevant velocities.

In addition to the GPR measurements, a multi-frequency FDEM Gem-2 survey was carried out using a Geophex GEM-2 system, with a scanning depth of several meters, and the ability to simultaneously transmit and record five frequencies corresponding to five penetration depths (Table 2; Figures 2, 4). The electromagnetic



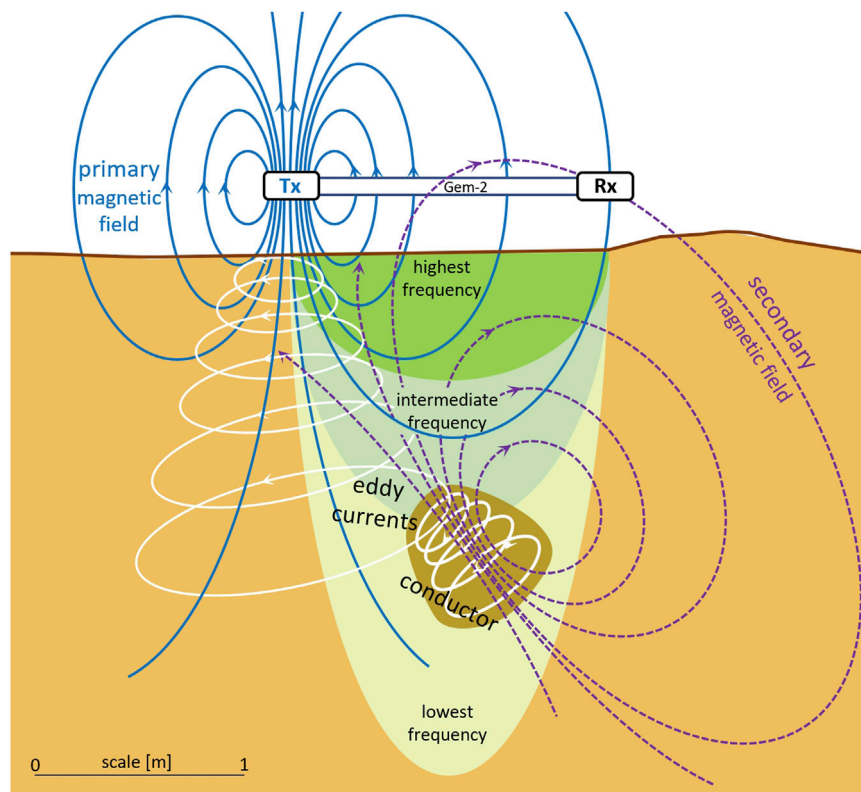


FIGURE 4

Multiple frequency FDEM Gem-2 Sounding scheme, reaching different depths of penetration: bulk EC integral from the surface to the penetration depth of the eddy currents at a certain frequency (modified from [Arcone, 1981](#)). The dimensions are typical to the results of our study.

system was held in a horizontal-dipole position to reduce penetration since the target was to assess the shallow subsurface at higher resolution; the depth was calculated using Eq. 10 ([Supplementary Appendix II](#)), based on our previous knowledge of the study area with adaptations for the subsurface model. The continuous subsurface scanning ensured similar conditions for all lines/locations. The sensor height above the surface was 1 m, corresponding to an average surface swath width of about 1 m from the surface. The HDR-GPR and FDEM subsurface scanning path was predefined by ground control points, registered by a differential GPS, with a spatial accuracy of ~ 1.0 cm. Samples were collected at intervals of 25 Hz along the predefined pathlines by walking with the instrument at ~ 2.5 km/h (± 0.5 m/s), resulting in an average of 50 measurements per meter profile length.

The FDEM data were filtered using a nonlinear filter to remove spikes and random/ambient noise. A spatial bandpass filter was applied for antialiasing. Based on the halfspace layered model, a normalized weighted algorithm was computed to create an inversion of the frequency interval for every two consecutive frequency pairs. The result is a series of EC maps integrating all EC data of a specific depth range between two frequency pairs ([Figure 4](#); [Table 2](#)). The selected algorithm is the proprietorship of GeoSense Ltd. In this paper, we present the analysis of the highest frequency, i.e., 62,525 Hz, which was used to measure the top meter of interest.

The integration of GPR and FDEM allowed us to assess the subsurface using two independent but complementary methods and explore various electromagnetic properties that enlarge the geophysical perspective. The FDEM enabled the spatial imaging of EC levels to a depth-range of 0.8–1.7 m, as a function of the electrical properties of the soil-rock layers and the concentration of dissolved salts, mainly sodium chloride (NaCl) and potassium chloride (KCl) in both hillslope types, and dissolved calcium carbonate (CaCO_3) in the heterogeneous hillslopes. The GPR allowed us to conduct 2D and 3D imaging dominated by the differences and variations in EMW propagation velocities and dielectric permittivities, distinguishing interfaces and changes in volumetric soil-water and rock-water content down to a depth of 1.4 m.

Results

GPR imaging

The results of the medium-resolution GX-750 MHz HDR-GPR imaging are presented in [Figures 6, 7](#). Two-dimensional wide-view GPR profiles of homogeneous vs heterogeneous plots are presented in [Figure 6](#) for depth-ranges of 0.0–1.2 m and 0.0–1.4 m, respectively. The homogeneous sections reveal relatively continuous and uniform reflections and returns, indicating

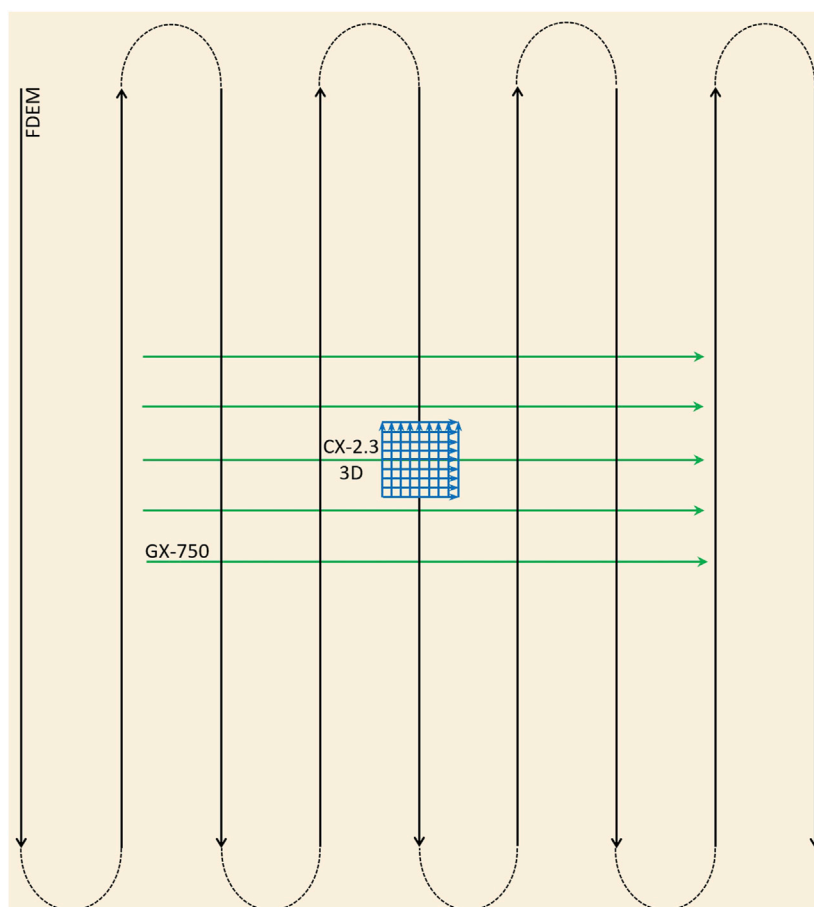


FIGURE 5 The top-view of 2D–3D GPR and FDEM imaging scheme of a characteristic measurement procedure plot in the Sayeret Shaked site. The black lines represent the Gem-2 FDEM profiles, the green lines represent the HDR GPR GX-750 MHz profiles, and the blue grid in the center represents the 3D GPR CX-2.3 GHz profiles.

TABLE 2 FDEM’s frequency (Hz) for effective penetration depth (m), with transmission frequencies utilized in this study, and the effective penetration depth. Values were calculated using Eqs 3, 4 and further explained in [Supplementary Appendix 1](#), with the adaptation for the horizontal dipole setting.

Penetration depth [m] (vertical dipole setting) for EC range of 30–140 mS/m					
EC [mS/m]	130	85			40
Frequency [Hz]	Minima	Minimum	Average	Maximum	Maxima
725	2.5	2.8	3.5	4.2	5.0
2,225	1.9	2.1	2.6	3.2	3.8
6,725	1.4	1.6	2.0	2.4	2.9
20,525	1.1	1.2	1.5	1.8	2.2
62,525	0.8	0.9	1.1	1.4	1.7

relatively uniform soil texture and water content throughout the layer. The soil-water content may override granular and soil-structural changes. At the same time, the heterogeneous sections are discontinuous and comprised of fractured/weathered chalky bedrock covered with a thin soil layer (~10 cm thickness).

Due to the different soil-rock propagation velocities of the GPR waves, the two hillslope types yielded two different depths per the same time-range (24 ns). The velocities of the EMW were measured from the various GPR profiles by analyzing diffractions—which are hyperbolic features in the images (for details concerning the velocity analysis

TABLE 3 The GPR and FDEM imaging parameters, settings, and the measured average EMW velocities for our study.

Geophysical system	HDR GPR GX-750	GPR CX-2.3	FDEM Gem-2
Center frequency	750 MHz	2.3 GHz	62,525 Hz
Sampling frequency	9.600 GHz	35.530 GHz	25 Hz
Step interval (m)	0.02	0.005	0.05
Time window (ns)	35	9	-
Stack	auto, typically ≥ 64	16	3
Average penetration depth range (m)	1.3–1.6	0.2–0.3	0.9–1.4
EMW velocity (soil: m/ns)	0.075–0.095 (± 0.005)	0.080–0.095 (± 0.005)	-
EMW velocity (rock: m/ns)	0.095–0.115 (± 0.005)	0.100–0.115 (± 0.005)	-

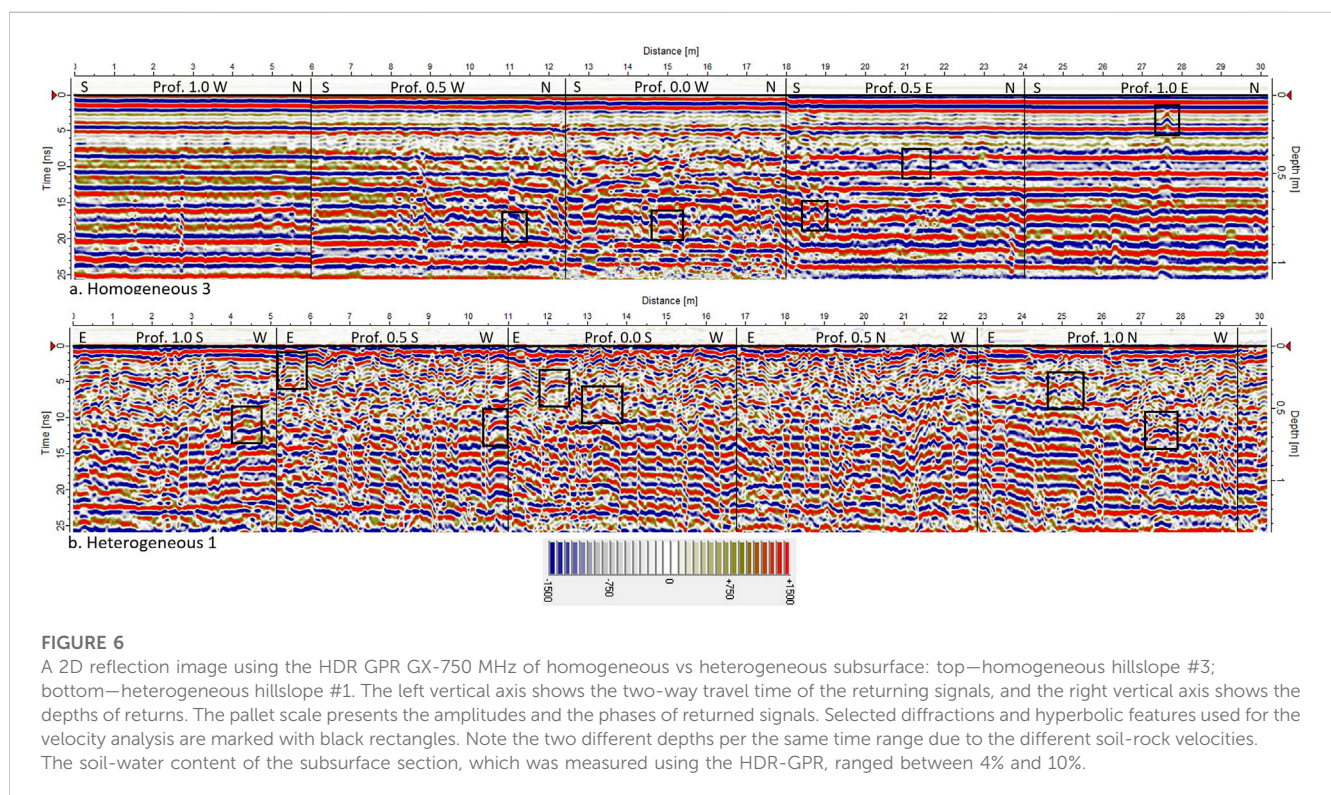


FIGURE 6
 A 2D reflection image using the HDR GPR GX-750 MHz of homogeneous vs heterogeneous subsurface: top—homogeneous hillslope #3; bottom—heterogeneous hillslope #1. The left vertical axis shows the two-way travel time of the returning signals, and the right vertical axis shows the depths of returns. The pallet scale presents the amplitudes and the phases of returned signals. Selected diffractions and hyperbolic features used for the velocity analysis are marked with black rectangles. Note the two different depths per the same time range due to the different soil-rock velocities. The soil-water content of the subsurface section, which was measured using the HDR-GPR, ranged between 4% and 10%.

process, see: Basson, 1992; Shamir et al., 2018)—yielded the following results: an average velocity of 0.08 m/ns ($\pm 5\%$) for the homogeneous, soily subsurface vs an average of 0.10 m/ns ($\pm 4\%$) for the heterogeneous, rocky subsurface. Higher average EMW velocity measured within a soil or rock layer indicates lower water content, while the lower average velocity of the same substance indicates higher water content. The different soil-rock velocities determine penetration depths per time range; penetration depth was ~ 1.10 m in the homogeneous subsurface and ~ 1.35 m in the heterogeneous subsurface.

The moisture content of subsurface soil layers was measured using HDR-GPR, ranging between 3% and 12%, which depended mainly on depth. The soil-water content in the heterogeneous chalky hillslopes varied between 7% and 9%, which encompasses a relatively narrow range. The accuracy of the water-content measurements is $\pm 2\%$.

A detailed comparison between the two hillslope types (homogeneous at the top; heterogeneous at the bottom) is presented in Figure 7, using two GX-750 MHz HDR GPR data processing procedures: the left images, with lower resolution, are more sensitive to absence of water in soil (note the stretch of the primary wavelength from ~ 0.55 m downwards as a result of this effect) (Basson, 1992; Shamir et al., 2018). The higher-resolution images on the right enhance the continuity of reflectors because of the low sensitivity to the irregular water content. The effective depth per 30 ns of the presented two-way time range is ~ 1.25 m. The right top image enhances the continuity of reflectors, representing a relatively massive layer of chalky bedrock to a depth of 1.25 m at the heterogeneous hillslope sections. The effective depth per the present 30 ns two-way time range of the heterogeneous subsurface is ~ 1.55 m.

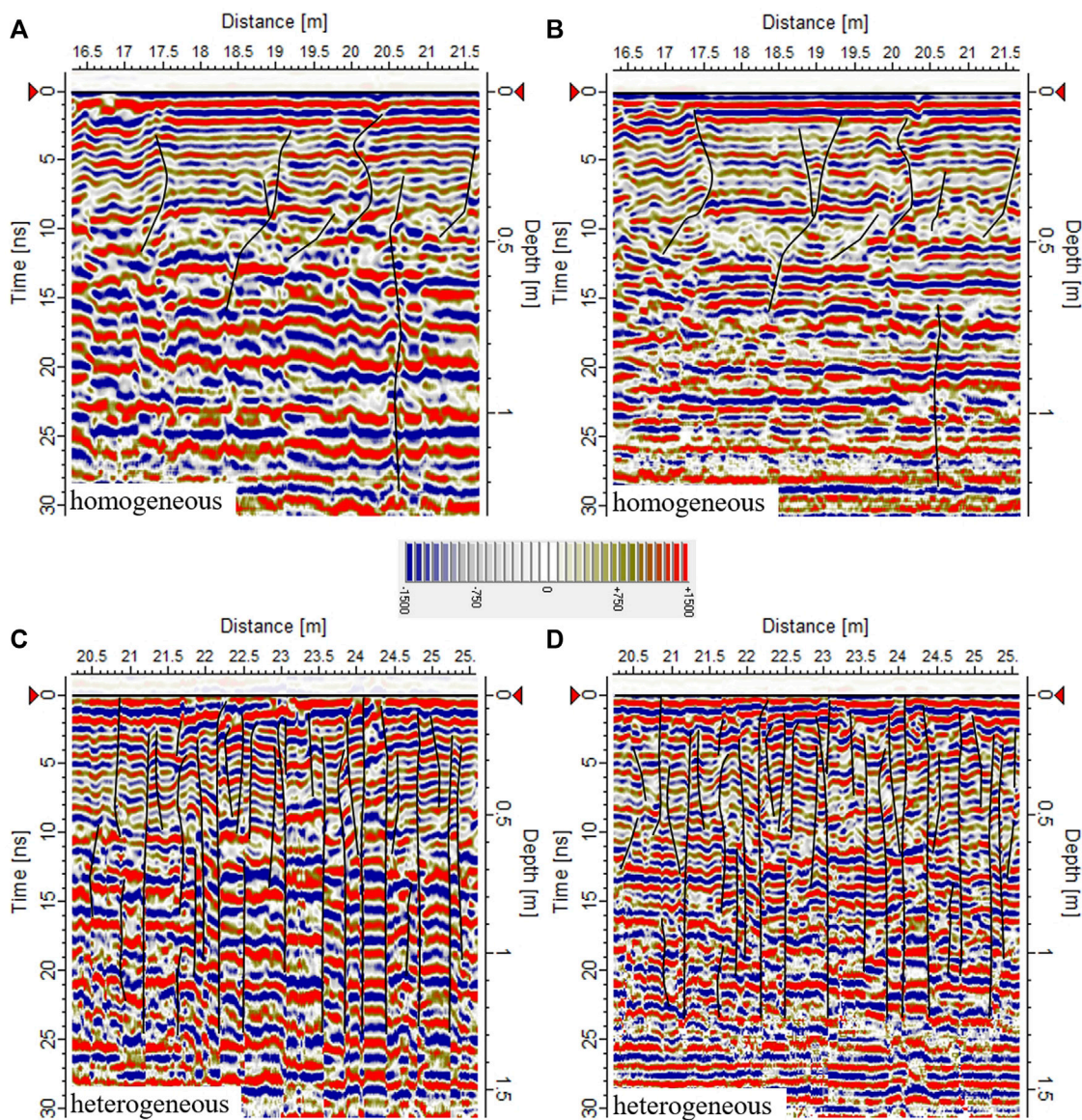


FIGURE 7
 GX-750 MHz HDR GPR profiles of homogeneous (A, B) and heterogeneous (C, D) hillslope sections in two data processing procedures: the left images present higher sensitivity to the absence of soil-water. The right images present a higher resolution that enhances the continuity of the reflectors. In both images, black lines represented major cracks in the subsurface. In both images, the homogeneous section appears relatively continuous with horizontal layers. Note the effective depth per the present 30 ns two-way time range of the heterogeneous subsurface is ~1.55 m while that of the homogeneous subsurface is ~1.25 m.

The results of the high-resolution CX-2.3 GHz GPR imaging of a very shallow part of the section (depth range of ~0.05–0.15 m) are presented in Figure 8. Three-dimensional depth slices and cross-sections at a depth of 0.05 m are presented for homogeneous vs heterogeneous subsurfaces. Similar to the color palette of Figures 6, 7, the strength and the phase of the EMW returns are represented by the strength of the red-blue colors. The homogeneous section is relatively continuous, while the heterogeneous one is discontinuous, starting at the top layer (0.05–0.15 m), and indicating the underlying fractured and weathered bedrock.

FDEM imaging

The shallowest FDEM measurements show EC variations between and within hillslope type. The average penetration depth varies from 0.8 m for the highest measured EC and 1.7 m for the lowest (Table 2). The EC imaging of homogeneous and heterogeneous hillslopes using the FDEM Gem-2 system (conducted at 62,525 Hz, horizontal mode) is presented in Figure 9. Substantial differences in EC were found between the homogeneous (the lower EC scale ~51–63 mS/m) and heterogeneous hillslopes (the medium-to-high part of the EC

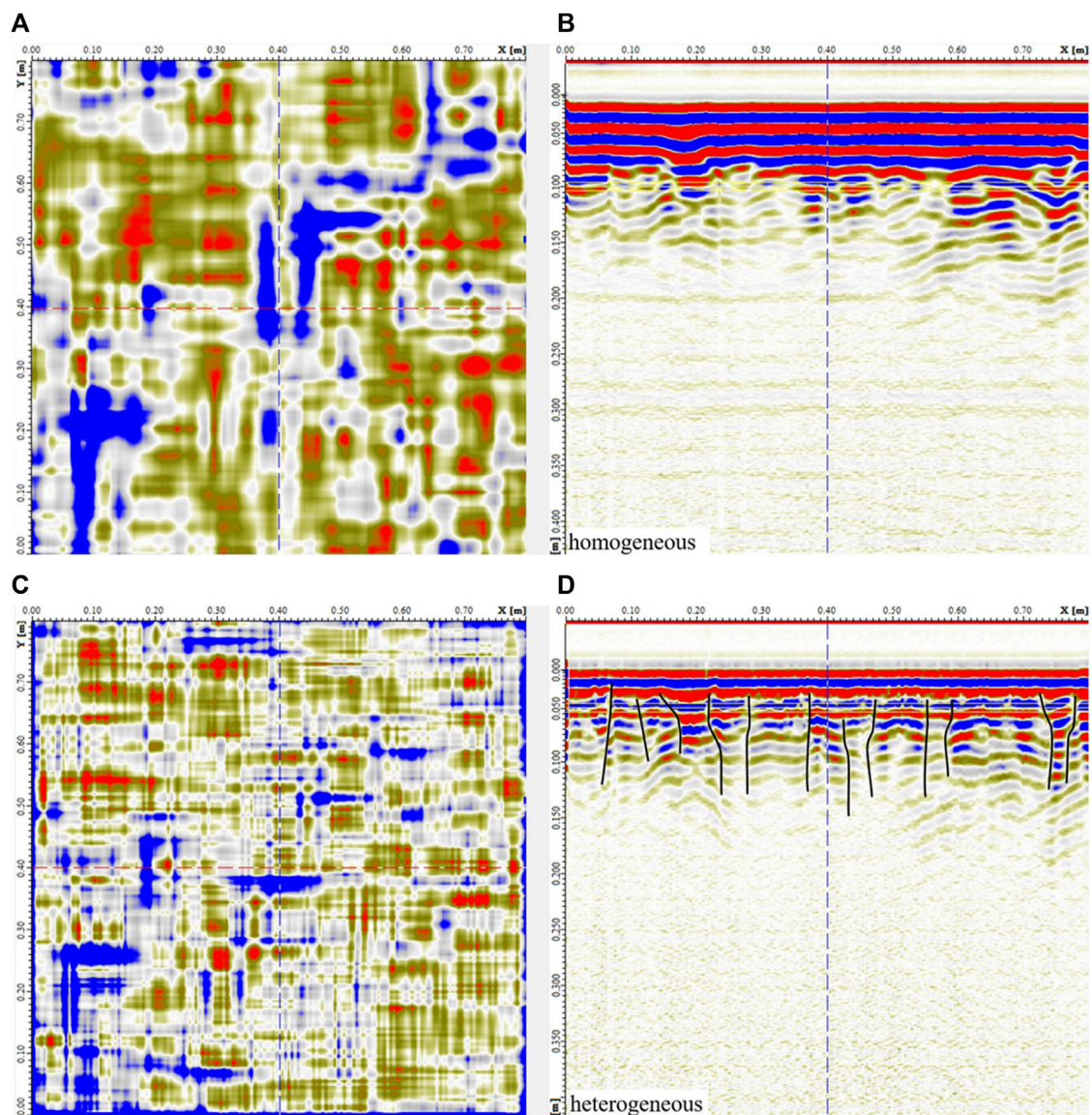


FIGURE 8

High-resolution CX-2.3 GHz GPR imaging of the homogeneous 3 (top) and the heterogeneous 3 (bottom) hillslopes. (A): Depth plane-slice view of a 0.8 m × 0.8 m plot at a depth of 0.10 m. (B): profile along $y = 0.40$ m. As shown by the depth slice and the profile, homogeneous hillslope #3 comprises typically non-stony, silty soil. Note that these images are valid for a centimeter scale. The backslope of heterogeneous hillslope #3 enhances the fracture visibility of the uppermost ~0.15 m. (C): Depth plane-slice view of a 0.8 m × 0.8 m plot at a depth of 0.05 m. (D): profile along $y = 0.40$ m. As shown at the depth slice and the profile, heterogeneous hillslope #3 comprises typically fractured chalk bedrock; major shallow cracks are marked in black. The CX-2.3 GHz GPR images show that the bedrock is only several centimeters below the surface in most of the heterogeneous hillslopes.

scale ~75–119 mS/m). Also, differences were found among the three heterogeneous hillslopes, as clearly seen in Figure 9. It should be noted that the results reflect the average EC of the entire column underneath the device.

Discussion

This geophysical study is a pioneer in exploring the subsurface characteristics to assess geodiversity in dryland ecosystems, using a unique complementary combination of 2D and 3D GPR and FDEM methods. The GPR methods yielded 2D and 3D reflection images

dominated by the differences and variations in dielectric permittivities, with differentiating layers and significant changes in soil-water content, which corresponds with the findings of Brevik et al. (2006). The top ~1.0–1.4 m were spatially imaged using the GX-750 MHz HDR GPR system, providing reflections that enable us to observe through soil-rock boundaries and layer interfaces, alongside variations in soil-water content. Specifically, it enabled to detect and image of the fractured and weathered bedrock. The high-resolution CX-2.3 GHz GPR imaging at the center areas allowed us to detect and observe 3D differences between the homogeneous and heterogeneous hillslopes in high resolution and assess the degree of micro-cracking in the bedrock.

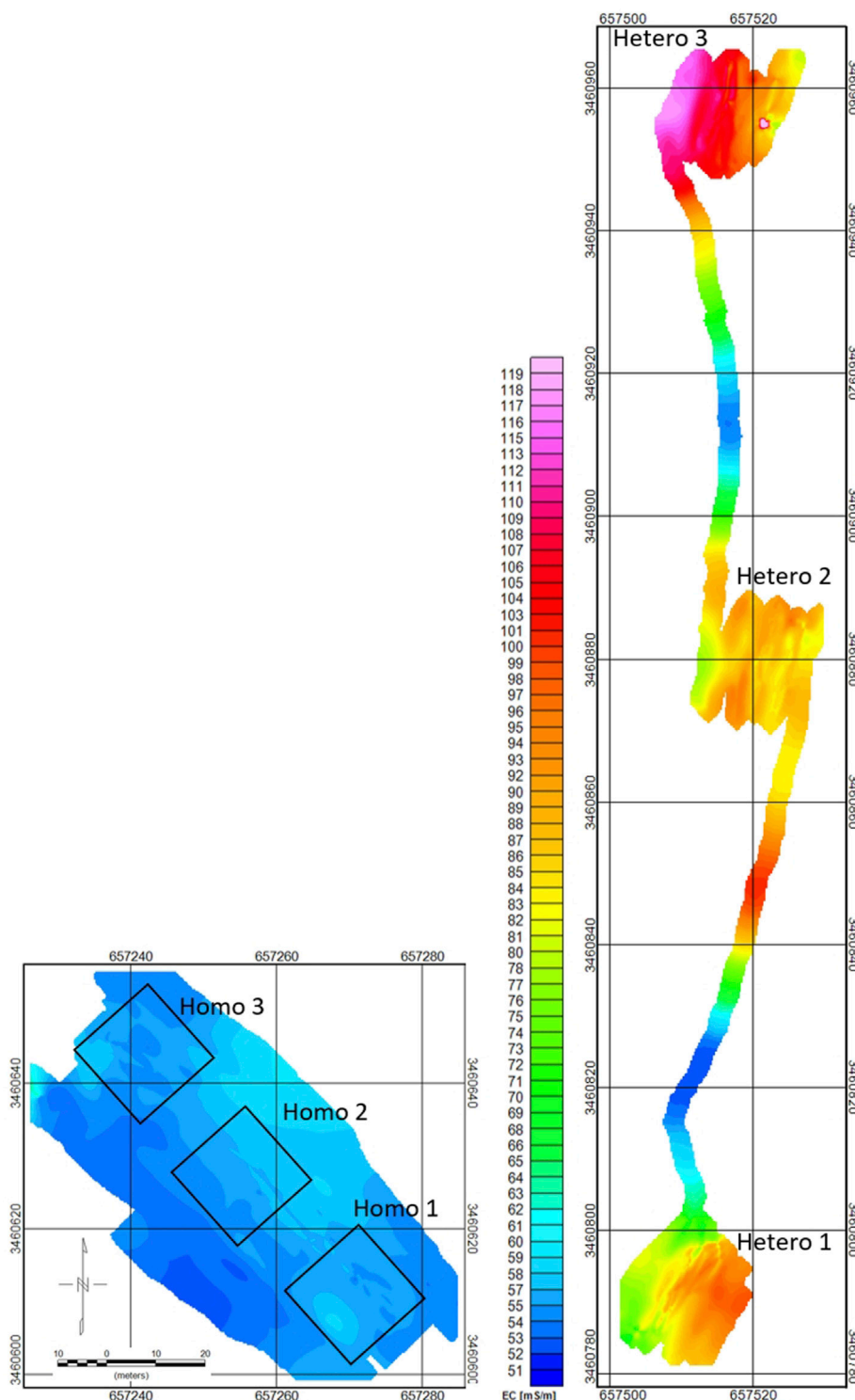


FIGURE 9

EC imaging of homogeneous and heterogeneous hillslopes using the Gem-2 FDEM system. The imaging was conducted using 62,525 Hz data (horizontal mode). The EC scales of the two zones are equal. The scale and north arrow are the same for both sites. The results show that EC is relatively uniform throughout the homogeneous hillslopes, i.e., variations of about 12 mS/m to an average depth range of ~1.3–1.5 m. At the same time, both within and among the heterogeneous hillslopes, variations in EC were almost four times greater, i.e., 44 mS/m in a depth range of 0.7–1.2 m, demonstrating the substantial variability of the heterogeneous hillslopes' landform. Also, greater EC variations of 64 mS/m in total can be seen between the higher conductive areas at the heterogeneous hillslopes and the pathways connecting the hillslopes. The accuracy of average EC level values presented in the FDEM images is ± 5.0 mS/m.

Simultaneously, the FDEM method provided a complete 3D imaging of the sites' apparent EC between a depth range of 0.8–1.7 m. The measured EC levels of the homogeneous and heterogeneous hillslopes were substantially different, and fit the results obtained in a recent study (Stavi et al., 2019). It appears that these differences, which are considerably greater than expected, are affected by the combination of two main parameters: 1) intrinsic EC of the soil-rock interface, and 2) the concentration of dissolved salts, mainly NaCl and KCl, and possibly dissolved CaCO₃ at the carbonatic heterogeneous hillslopes, which act as electrolytes that highly increase the total EC.

The substantial differences in EC values between the homogeneous and heterogeneous hillslopes are due to different properties of the soil-rock interface, alongside differences in soil-water and salt contents and their intrinsic ability to retain water remnants. In semiarid and arid areas, since soil-water is far from saturation, the ground salts are generally in the form of solids, i.e., act as isolators for electrical currents. When the soil-water content increases, it dissolves the salts, transforming the soil-water into an electrolyte. Therefore, higher soil-water is represented by higher EC. An important insight of this study is that in the heterogeneous hillslopes, the shrubs thrive despite the high salinity when coupled with high-moisture pockets or micro-aquicludes in the fractured bedrock, which alleviate the risk imposed by the comparatively high salinity conditions (Stavi et al., 2018a; Stavi et al., 2019). This accords with the study hypothesis and fits results obtained in previous studies that showed high cover, vitality, richness, and diversity of shrubs in the heterogeneous hillslopes, as opposed to low values of these vegetative parameters coupled with high die-off rates of shrubs in the homogeneous hillslopes (Stavi et al., 2018a; Stavi et al., 2019; Stavi et al., 2021a; Stavi et al., 2021b). As such, this study complements an important knowledge gap regarding the mechanism that regulates the vitality of shrubs in this environment under severe drought episodes. To some extent, this also accords with McCormick et al. (2021), who proposed that the availability of bedrock-water storage may be key in predicting large-scale dynamics of woody vegetation under climate change. The forecasted climatic change, with increasing aridity and expansion of dryland areas (Huang et al., 2016), makes the insights of this study relevant for other parts of the world.

Conclusion

Geophysical exploration in a semiarid LTER in the northwestern Negev drylands reveals the differences in the subsurface of two hillslope types: homogeneous hillslopes with continuous silty loam layers vs heterogeneous hillslopes with fractured and weathered chalky bedrock. The soil-water content of the heterogeneous hillslopes was much greater than that in the homogeneous hillslopes. This difference can be explained by the high-moisture pockets or micro-aquicludes found in the heterogeneous hillslopes, which enable shrubs to survive and thrive under long-term drought episodes. At the same time, the absence of such pockets in the homogeneous hillslopes leads to shrub die-off when climatic conditions change abruptly. Further, the higher soil-water availability in the heterogeneous hillslopes seems to mitigate the stress imposed by the relatively high soil salinity conditions.

Data availability statement

The raw data supporting the conclusions of this article will be made available by the authors, without undue reservation.

Ethics statement

Written informed consent was obtained from the individual(s) for the publication of any identifiable images or data included in this article.

Author contributions

UB—formulated the study, operated the GPR and the FDEM/data collection, conducted the data processing and interpretation, wrote the article. AR—design the study, participated in writing the article. HY—design the study, participated in writing the article. XC—design the study, participated in writing the article, obtained the funding. ZX—design the study, participated in writing the article. IS—design the study, participated in writing the article, obtained the funding. All authors contributed to the article and approved the submitted version.

Acknowledgments

The study was funded by the Joint Program of the Israel Science Foundation (ISF: Grant No. 3257/20) and the National Natural Science Foundation of China (NSFC: Grant No. 32061143014). The Dead Sea and Arava Science Center is supported by the Israel Ministry of Science and Technology. The authors are grateful to Michelle Finzi for proofreading of the manuscript. The authors acknowledge the very helpful comments made by two reviewers, which enabled the meaningful improvement of the manuscript's original version.

Conflict of interest

Author UB was employed by the company GeoSense Ltd.

The authors declare that the research was conducted in the absence of any commercial or financial relationships that could be construed as a potential conflict of interest.

Publisher's note

All claims expressed in this article are solely those of the authors and do not necessarily represent those of their affiliated organizations, or those of the publisher, the editors and the reviewers. Any product that may be evaluated in this article, or claim that may be made by its manufacturer, is not guaranteed or endorsed by the publisher.

Supplementary material

The Supplementary Material for this article can be found online at: <https://www.frontiersin.org/articles/10.3389/fenvs.2023.1168104/full#supplementary-material>

References

- Alahuhta, J., Ala-Hulkko, T., Tukiainen, T., Purola, P., Akujärvi, A., Lampinen, R., et al. (2019). The role of geodiversity in providing ecosystem services at broad scales. *Ecol. Indic.* 91, 47–56. doi:10.1016/j.ecolind.2018.03.068
- Arcone, S. A. (1981). *Some field studies of the correlation between electromagnetic and direct current measurements of ground resistivity. Underground correlation*, ASTM STP 741. West Conshohocken, Pennsylvania, United States: American Society for Testing and Materials, 92–110.
- Argaman, E., Barth, R., Moshe, Y., and Ben-Hur, M. (2020). Long-term effects of climatic and hydrological variation on natural vegetation production and characteristics in a semi-arid watershed: The northern Negev, Israel. *Isr. Sci. Total Environ.* 747, 141146. doi:10.1016/j.scitotenv.2020.141146
- Astm International (2023a). *Standard guide for using the frequency Domain electromagnetic method for subsurface investigations*. ASTM D6639-01 (West Conshohocken, PA, USA: ASTM International).
- Astm International (2023b). *Standard guide for using the frequency Domain electromagnetic method for subsurface site characterizations*. ASTM D6639-18 (West Conshohocken, PA, USA: ASTM International).
- Astm International (2023c). *Standard guide for using the surface ground penetrating radar method for subsurface investigation*. ASTM D6432-19 (West Conshohocken, PA, USA: ASTM International).
- Baruch, Y., Basson, U., Nachum, O., and Riech, R. (2021). Robinson's arch: Results of a geophysical study. City of david studies of ancient jerusalem. *Eyal Meiron, Megalim Inst. - City David, Jerus. Eulul* 16.
- Basson, U., Ben-Avraham, Z., Garfunkel, Z., and Lyakhovsky, V. (2002). Development of recent faulting in the southern Dead Sea Rift according to GPR imaging. *Tectonophys. Eur. Geophys. Soc. (EGS) Stephan Mueller Spec. Publ. Ser.* 2, 35–48. doi:10.5194/smsps-2-35-2002
- Basson, U. (2017). *Detection of the continuation of the Herodian Street through the underground sewage tunnel using ground penetration radar imaging*. GeoSense report 0125052017. Battlies Green, England: GeoSense.
- Basson, U., Enzel, Y., Amit, R., and Ben-Avraham, Z. (1994). Detecting and mapping recent faults with a ground penetrating radar in the alluvial fans of the Arava valley, Israel. *Kitchener, Ont* 2, 777–788. doi:10.3997/2214-4609-pdb.300.57
- Basson, U., and Ginzburg, A. (2008). Mapping archaeological remains at the Banias using ground penetrating Radar (GPR). *Banias IAA Rep 38, Paneas II Finds Other Stud.* 189–193.
- Basson, U. (2021). Ground penetrating radar imaging of the western wall. *New Stud. Archaeol. Jerus. its Region* 14, 65–88.
- Basson, U. (2000). *Imaging of active fault zone in the Dead Sea rift: Evrona fault zone as a case study*. A thesis submitted for the degree of Ph.D. (Tel Aviv, Israel: Tel-Aviv University), 195.
- Basson, U. (1992). "Mapping of moisture content and structure of unsaturated sand layers with ground penetrating radar," A thesis submitted for the degree of Master of Sciences in Geophysics (Tel Aviv, Israel: Tel-Aviv University), 80.
- Basson, U. (2023). "The thickness of the western wall ground penetrating radar imaging," in *The southern Wall and Corners of the temple mount: Past, present, future (ancient jerusalem publications 1)*. Editors Y. Baruch, R. Reich, M. Hagbi, and J. Uziel (Jerusalem, Israel: University Park-Jerusalem), 491–508.
- Ben-Dor, E., Metternicht, G., Goldshleger, N., Eshel, M., Mirilas, V., and Basson, U. (2008). "Review of remote sensing based methods to assess soil salinity," in *Remote sensing of soil salinization – impact and land management*. Editors G. Metternicht and A. Zinck (Boca Raton, FL, USA: CRC Press), 39–60.
- Bétard, F., and Peulvast, J. P. (2019). Geodiversity hotspots: Concept, method and cartographic application for geoconservation purposes at a regional scale. *Environ. Manage.* 63. doi:10.1007/s00267-019-01168-5
- Brevik, E. C., Fenton, T. E., and Lazari, A. (2006). Soil electrical conductivity as a function of soil water content and implications for soil mapping. *Precis. Agric.* 7. doi:10.1007/s11119-006-9021-x
- Calvo-Cases, A., Arnau-Rosalén, E., Boix-Fayos, C., Estrany, J., Roxo, M. J., and Symeonakis, E. (2021). Eco-geomorphological connectivity and coupling interactions at hillslope scale in dryland: Concepts and critical examples. *J. Arid. Environ.* 186, 104418. doi:10.1016/j.jaridenv.2020.104418
- Crisp, J. R., Ellison, J. C., Fischer, A., and Tan, J. S. (2022). Geodiversity inclusiveness in biodiversity assessment. *Progr. Phys. Geogr.* 47. doi:10.1177/03091333221122292
- Davis, E. A. (1977). "Root system of shrub live oak in relation to water yield by chaparral," in *Proceedings of the Meetings of the Arizona Section of the American Water Resources Association and the Hydrology Section of the Arizona Academy of Science*, Las Vegas, NV, USA.
- Davis, J. L., and Annan, A. P. (1989). Ground penetrating radar for high resolution mapping of soil and rock stratigraphy. *Geophys. Prospect* 37, 531–551. doi:10.1111/j.1365-2478.1989.tb02221.x
- dos Santos, D. S., Mansur, K. L., de Arruda, E. R., Dantas, M. E., and Shinzato, E. (2019). Geodiversity mapping and relationship with vegetation: A regional-scale application in SE Brazil. *Geoh Heritage* 11. doi:10.1007/s12371-018-0295-y
- EcoPeace Middle East (2019). Climate change, water security, and national security for Jordan, Palestine, and Israel, Tel Aviv. EcoPeace Middle East. <https://reliefweb.int/sites/reliefweb.int/files/resources/climate-change-web.pdf>.
- Ginat, H., and Zilberman, E. (1991). Structural and morphological development of the udva valley. *Isr. J. Earth Sci.* 40, 209–218.
- Goldshleger, N., Basson, U., Fastig, S., and Azaria, I. (2018). Using combined close-range active and passive-remote sensing methods to detect sinkholes. *J. Remote Sens. GIS* 7, 1000222. doi:10.4172/2469-4134.1000222
- Goldshleger, N., and Basson, U. (2016a). Identification of sewage leaking by remote sensing methods. *Geophys. Res. Abstr.* 18, EGU2016. doi:10.4172/2469-4134.1000222
- Goldshleger, N., and Basson, U. (2016b). "Utilization of ground-penetrating radar and frequency Domain electromagnetic for investigation of sewage leaks," in *Environmental applications of remote sensing*. Editor M. Marghany (London, UK: IntechOpen), 261–280. doi:10.5772/62156
- Goldshleger, N., Shamir, O., Basson, U., and Zaady, E. (2019). Frequency Domain Electromagnetic Method (FDEM) as a tool to study contamination at the sub-soil layer. *Geosciences* 9, 382. doi:10.3390/geosciences9090382
- Gray, M. (2005). "Geodiversity and geoconservation: What, why, and how?" in *Geodiversity and geoconservation*, 22. Editor V. L. Santucci (Hancock, MI: The George Wright Forum), 4–12.
- Hahm, W. J., Rempe, D. M., Dralle, D. N., Dawson, T. E., and Dietrich, W. E. (2020). Oak transpiration drawn from the weathered bedrock vadose zone in the summer dry season. *Water Resour. Res.* 56, e2020WR027419. doi:10.1029/2020WR027419
- Hellmers, H., Horton, J. S., Juhren, G., and O'Keefe, J. (1955). Root systems of some chaparral plants in southern California. *Ecology* 36, 667–678. doi:10.2307/1931305
- Herr, N., Shani, U., and Riou, J. (2016). The water budget dynamics in rock-soil-tree system in Quercus ithaburensis forest-park and Quercus calliprinos scrub. *Ecol. Environ.* 7, 64.
- Huang, H. (2005). Depth of investigation for small broadband electromagnetic sensors. *Geophysics* 70, 135–142. doi:10.1190/1.2122412
- Huang, H., and Won, I. J. (2003). Real-time resistivity sounding using a handheld broadband electromagnetic sensor. *Geophysics* 68, 1224–1231. doi:10.1190/1.1598114
- Huang, J., Yu, H., Guan, X., Wang, G., and Guo, R. (2016). Accelerated dryland expansion under climate change. *Nat. Clim. Change* 6, 166–171. doi:10.1038/nclimate2837
- Ibáñez, J. J., Pérez-Gómez, R., Ganis, P., and Feoli, E. (2016). The use of vegetation series to assess α and β vegetation diversity and their relationships with geodiversity in the province of Almería (Spain) with watersheds as operational geographic units. *Plant Biosyst* 150, 1395–1407. doi:10.1080/11263504.2016.1165755
- Lazar, M., Basson, U., Ben-David, R., and Coddington, J. (2021). When faults diverge – high resolution imaging of an intra-fault zone in an urban environment. A case study from the city of Tiberias, Israel. *Eng. Geol.* 296, 106454. doi:10.1016/j.enggeo.2021.106454
- Lazar, M., Basson, U., Levy, T. E., and Landau, A. Y. (2020). The door to Dor: Tracing unseen anthropogenic impact in an ancient port. *Geoarchaeology* 2020, 1–10. doi:10.1002/zea.21825
- Lazar, M., Engoltz, K., Basson, U., and Yasur-Landau, A. (2018). Water saturated sand and a shallow bay: Combining coastal geophysics and underwater archaeology in the south bay of tel dor. *Qua. Int.* 473. doi:10.1016/j.quaint.2017.02.025
- Marco, S., Agnon, A., Ellenblum, R., Eidelman, A., Basson, U., and Boas, A. (1997). 817-Year-old walls offset sinistrally 2.1 m by the Dead Sea transform, Israel. *J. Geodyn.* 24, 11–20. doi:10.1016/S0264-3707(96)00041-5
- McCormick, E. L., Dralle, D. N., Hahm, W. J., Tune, A. K., Schmidt, L. M., Chadwick, K. D., et al. (2021). Widespread woody plant use of water stored in bedrock. *Nature* 597, 225–229. doi:10.1038/s41586-021-03761-3
- Shachak, M. (2011). Ecological textures: Ecological systems in the northern Negev as a model. *Ecol. Environ.* 1, 18–29.
- Shamir, O., Goldshleger, N., Basson, U., and Reshef, M. (2018). Laboratory measurements of subsurface spatial moisture content by Ground-Penetrating Radar (GPR) diffraction and reflection imaging of agricultural soils. *Remote Sens.* 10, 1667. doi:10.3390/rs10101667
- Sher, Y., Zaady, E., Ronen, Z., and Nejidat, A. (2012). Nitrification activity and levels of inorganic nitrogen in soils of a semi-arid ecosystem following a drought-induced shrub death. *Eur. J. Soil Biol.* 53, 86–93. doi:10.1016/j.ejsobi.2012.09.002
- Spies, B. R. (1989). Depth of investigation in electromagnetic sounding methods. *Geophysics* 54, 872–888. doi:10.1190/1.1442716
- Stavi, I., Rachmilevitch, S., Hjazin, A., and Yizhaq, H. (2018a). Geodiversity decreases shrub mortality and increases ecosystem tolerance to droughts and climate change. *Earth Surf. Proc. Land.* 43, 2808–2817. doi:10.1002/esp.4412
- Stavi, I., Rachmilevitch, S., and Yizhaq, H. (2019). Geodiversity effects on soil quality and geo-ecosystem functioning in dryland. *Catena* 176, 372–380. doi:10.1016/j.catena.2019.01.037

- Stavi, I., Rachmilevitch, S., and Yizhaq, H. (2018b). Small-scale geodiversity regulates functioning, connectivity, and productivity of shrubby, semi-arid rangelands. *Land Degrad. Dev.* 29, 205–209. doi:10.1002/ldr.2469
- Stavi, I., Yizhaq, H., Szitenberg, A., and Zaady, E. (2021a). Patch-scale to hillslope-scale geodiversity alleviates susceptibility of dryland ecosystems to climate change: Insights from the Israeli Negev. *Curr. Opin. Environ. Sustain.* 50, 129–137. doi:10.1016/j.cosust.2021.03.009
- Stavi, I., Zaady, E., Gusarov, A., and Yizhaq, H. (2021b). Dead shrub patches as ecosystem engineers in degraded dryland. *J. Geogr. Sci.* 31, 1187–1204. doi:10.1007/s11442-021-1892-2
- Sudduth, K. A., Kitchen, N. R., Wiebold, W. J., Batchelor, W. D., Bollero, G. A., Bullock, D. G., et al. (2005). Relating apparent electrical conductivity to soil properties across the north-central USA. *Comput. Electron. Agric.* 46, 263–283. doi:10.1016/j.compag.2004.11.010
- Summers, J. K., Smith, L. M., Fulford, R. S., and de Jesus Crespo, R. (2018). “The role of ecosystem services in community well-being,” in *Ecosystem services and global ecology*. Editor L. Hufnagel (London, UK: IntechOpen), 145–168. doi:10.5772/intechopen.74068
- Thomas, M. F. (2012). Geodiversity and landscape sensitivity: A geomorphological perspective. *Scott. Geogr. J.* 128, 195–210. doi:10.1080/14702541.2012.725863
- Ulriksen, C. P. F. (1982). *Application of impulse radar to civil engineering*. Ph.D. thesis. (Lund: Univ. Technology).
- Ward, S. H., and Hohmann, G. W. (1988). “Electromagnetic theory for geophysical applications,” in *Electromagnetic methods in applied geophysics*. Editor M. N. Nabighian (Houston, Texas, United States: Society of Exploration Geophysicists), 130–311. doi:10.1190/1.9781560802631.ch4
- Widess, M. B. (1973). How thin is this bed? *Geophysics* 38, 1176–1180. doi:10.1190/1.1444043
- Won, I. J., Keiswetter, D. A., Fields, G. R. A., and Sutton, L. C. (1996). GEM-2: A new multi-frequency electromagnetic sensor. *J. Environ. Eng. Geophys.* 1, 129–137. doi:10.4133/JEEG1.2.129
- Yilmaz, O. (1987). “Seismic data processing,” in *Series: Investigation in geophysics 2*. Editor S. M. Doherty (Houston, Texas, United States: Society of Exploration Geophysicists).
- Zaady, E., Shir, Y., Ronen, Z., and Nujedat, A. (2012). The effect of consecutive drought in the northern Negev on soil characteristics and plant mortality. *Ecol. Environ.* 3, 44–52.